pH-activatable Ruthenium(II) Fluorescein Salphen Schiff Base Photosensitizers for Theranostic Applications

Martin Gillard,† Ludovic Troian-Gautier,† Anabelle Decottignies‡ and Benjamin Elias*,†

† Université catholique de Louvain (UCLouvain), Institut de la Matière Condensée et des Nanosciences (IMCN), Molecular Chemistry, Materials and Catalysis (MOST), Place Louis Pasteur 1, bte L4.01.02, B-1348 Louvain-la-Neuve, Belgium

‡ Université catholique de Louvain (UCLouvain), Genetic and Epigenetic Alterations of Genomes, de Duve Institute, Avenue Hippocrate 75, 1200 Brussels, Belgium

ABSTRACT: Ruthenium (II) polypyridyl complexes exhibit a lack of selectivity towards cancer tissues despite extensive studies as photosensitizers for photodynamic therapy (PDT). Here, we report pH-activatable Ru (II) photosensitizers for molecular targeted PDT by exploiting the higher acidity of tumoral tissue. The fluorescein moiety, well-known for its high pH sensitivity, was connected to a Ru center to yield novel photosensitizers for pH-sensitive $^1O_2$ photogeneration. Their ability to photosensitize molecular dioxygen was studied at various pHs and revealed a drastic enhancement from 0.07 to 0.66 of the $^1O^2$ quantum yield in acidic conditions (pH 7.5 to pH 5.5). Their photo-cytotoxicity against U2OS osteosarcoma cells was also investigated at pH 5.5 and 7.5 through IC_{50} determination. A strong enhancement of the photocytotoxicity reaching 880 nM was observed at pH 5.5 which showed the potential of such photosensitizers for pH-activatable PDT.

INTRODUCTION

The quest for more targeted photo-chemotherapeutics stimulated the search for new solutions to either locate the photosensitizer (PS) at the cancer cell or to make it more effective in tumoral tissues.[1] Among the different pathways explored, the increased acidity of tumors (pH 5.5-6.5 *vs.* 7.2-7.4 in healthy tissues) is very promising and has led to the development of new, promising therapies.[2] This includes the development of tumour antigen-targeted pH-sensitive antibodies, pH-responsive nanoparticle conjugates with anticancer drugs and a combination of alkaline diet through bicarbonate therapy to neutralize the tumoral tissue acidity.[3] Along with these innovative approaches, the quest for more targeted PDT agents has encouraged the study of a new class of PSs able to preferentially produce $^1O_2$ in cancer tissue based on their slightly higher acidity than healthy ones.[4] This would increase the accuracy of PDT activation and could open the way for PDT treatment of cancers at the metastatic stage, as suggested by a recent study.[5] Indeed, in pH activatable PDT, the fact that the PS is effective only in the more acidic cancer tissue allows for a wider zone of irradiation, containing both cancer and healthy tissue. Hence, the damage to the healthy cells is limited, which is the main drawback in the treatment of metastases. Some porphyrin and BODIPY derivatives have already been studied for pH-responsive PDT and showed very promising results *in cellulo* with enhanced photo-cytotoxicity against cancer cells in acidic conditions. Significantly different pH-dependent photocytotoxicities were reported for BODIPY dyes over HeLa cells (IC_{50} = 30 nM and 150 nM at pH 5.5 and 7.5 respectively). However, this class of compounds also show high toxicity in the dark with IC_{50} values in the micromolar range.[6] Concerning the porphyrin derivatives, either polypyridyl or amino substituents were added to the porphyrin core giving rise to intramolecular electron transfer that quenches the triplet excited state of porphyrin and prevents $^1O_2$ generation. The electron transfer can thus be suppressed by protonation in acidic conditions and the porphyrin's PDT activity is then restored along with the fluorescence and light absorption. Even if exhibiting very promising results such photocytotoxicities in the micromolar range, the pH-activatable porphyrins still show the drawbacks of porphyrin PDT agents which are a challenging synthesis, limited solubility, and high cytotoxicity in the dark.[7, 8, 9] Ru^{II} complexes are another class of PS that has been widely explored for various biological applications.[10] They often present lower cytotoxicity in the dark than BODIPY derivatives, as well as higher solubility and easier synthesis than porphyrins.[11] However, their potential as pH-activatable PDT agents has still not yet been widely investigated. Papish and co-workers paved the way for this approach by developing pH and light activated Ru^{II} polypyridyl complexes based on acid promoted photo-dissociation of ligands, also called pH-Activated Metallo Prodrugs (phAMP's), hence requiring higher concentrations of photoactivated complex.[12] Here, we aim at combining the PDT capabilities of Ru^{II} polypyridyl complexes with the well-known high pH sensitivity of fluorescein which was already reported as a marker of acidity for biological applications.[13] This, with a view of developing pH-activatable PDT agents of a new type. The Ru^{II} salphen Schiff base complex $[Ru(phen)_2dfsa]^{2+}$ **1** (dfsa = 5,6-difluoresceindiimine-1,10-phenanthroline) that contains two fluorescein moieties is the main studied candidate (**Figure 1**). $[Ru(phen)_3]^{2+}$ and fluorescein were used as reference compounds for the study. The Ru^{II} salphen Schiff base complex $[Ru(phen)_2salphen]^{2+}$ **3** and $[Ru(phen)_2mfsa]^{2+}$ **2** (mfsa = 5-monofluoresceindiimine-1,10-phenanthroline), which is the mono-fluorescein analogue of complex **1** were also prepared for comparison purposes. Singlet oxygen photosensitization was studied as a function of pH which revealed a drastic 10-fold enhancement of the $^1O_2$ quantum yield (from 0.07 to 0.66) in slightly acidic conditions (pH 5.5) compared to the physiological conditions (pH 7.5). The impact of acidity on the cell internalization and location of the complex was studied on the U2OS osteosarcoma cell line using confocal microscopy. Finally, the photocytotoxic activity of the complex was measured *in cellulo* at pH 7.5 and 5.5 and showed a substantial decrease of the IC_{50}, reaching 0.88 μM at pH 5.5.

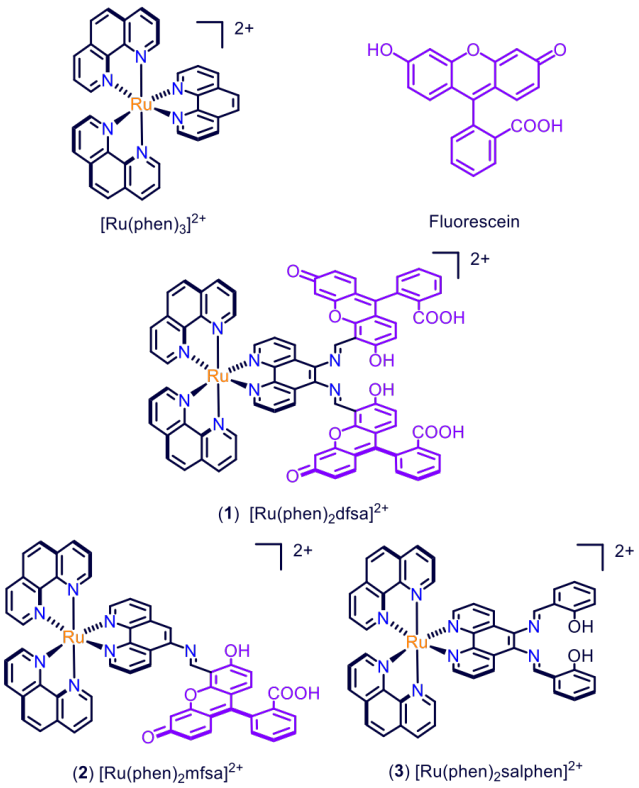

Figure 1. Structures of [Ru(phen)$_3$], fluorescein and of the Ru^{II} complexes **1**-**3**.

Results and discussions

Synthesis

The synthesis of a new Schiff base type ligand containing the fluorescein moiety (dfsa) was performed by condensing 5,6-diamino-1,10-phenanthroline with two equivalents of fluorescein-5-carbaldehyde. The aldehyde was itself obtained via a modified Reimer-Tiemman reaction,[14] in the presence of a catalytic amount of acetic acid in refluxing ethanol and was obtained with a 31% yield. A mono fluorescein analogue of the ligand (mfsa) was prepared from 5-amino-1,10-phenanthroline using similar conditions with a 42% yield. The structure of the ligands was confirmed by ^{1}H-NMR spectroscopy and HRMS analysis (see SI). The corresponding Ru^{II} complexes **1** and **2** depicted in **Figure 1** were synthesized by the direct chelation of the ligands onto a [Ru(phen)$_2$Cl$_2$] precursor in refluxing ethanol to yield the corresponding complexes as orange powders in 52-60% yields. Concerning complex **1**, ^{1}H-NMR spectroscopy unambiguously shows the symmetry of the compounds, which induces the equivalence of (i) the protons of the ligands and (ii) of the phenanthroline moieties which was not the case for the dissymmetric complex **2** (see SI).

Photophysical properties and pH dependence.

Light absorption data of **1** were recorded at ambient temperature in acetonitrile under air and in deionized water and are presented along with the data collected for the compounds **2**, **3**, [Ru(phen)$_3$]$^{2+}$ and fluorescein (**Table 1**). As depicted in **Figure 2**, the absorption spectrum of **1** in acetonitrile displayed the typical shape and molar absorption coefficients of Ru^{II} polypyridyl complexes such as the reference compound [Ru(phen)$_3$]$^{2+}$. Indeed, in the visible part of the spectra (at *ca.* 460 nm), absorption bands ($\varepsilon \approx$ 15000-25000 L.mol^{-1}.cm^{-1}) assigned to metal to ligand charge transfer (MLCT) transitions, were monitored. Strong absorption bands resulting from LC transitions centred on the phenanthroline ligands were also observed in the UV-region (250 nm), as for [Ru(phen)$_3$]$^{2+}$ and **1**. In acetonitrile, the presence of the two fluorescein moieties in **1** only leads to a relatively weak increase of the visible light absorption compared to [Ru(phen)$_3$]$^{2+}$ but showed a noticeable red shift of the MLCT transitions (from 447 nm in [Ru(phen)$_3$]$^{2+}$ to 459 nm in **1**). This was attributed to (i) the greater conjugation of the dfsa ligand compared to a phen and (ii) the presence of the two electron withdrawing imines in the dfsa ligand.

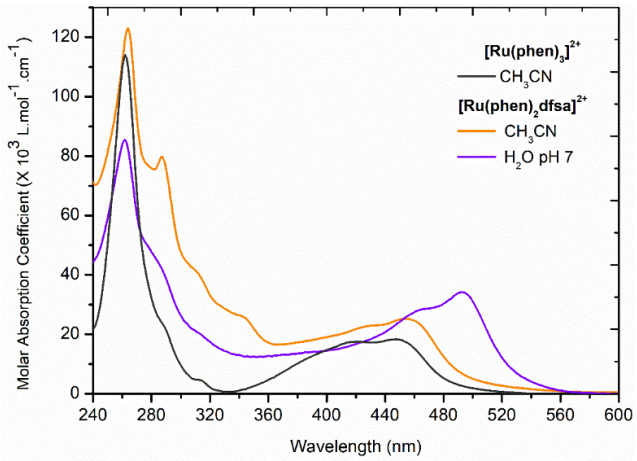

Figure 2. UV-visible absorption spectra of [Ru(phen)$_3$]$^{2+}$ in acetonitrile and of [Ru(phen)$_2$dfsa]$^{2+}$ **1** in acetonitrile and in deionized water at pH 7.

Table 1 - Absorption data in CH$_3$CN and in deionized H$_2$O.

Complex	Absorption λ_{max} [nm] (ε [10^3 L.mol^{-1}.cm^{-1}])[a]	
	CH$_3$CN	Deionized H$_2$O
[Ru(phen)$_3$]$^{2+}$	263, 447 (18.4)	263, 447 (18.4)
Fluorescein	453, 474 (11.8)	490 (67.3)
[Ru(phen)$_2$dfsa]$^{2+}$ **1**	264, 459 (24.8)	262, 493 (34.1)
[Ru(phen)$_2$mfsa]$^{2+}$ **2**	265, 456 (18.2)	262, 492 (22.1)
[Ru(phen)$_2$salphen]$^{2+}$ **3**	265, 458 (10.4)	265, 458 (10.8)

[a] Measurements were performed with 1 x 10^{-5} mol L^{-1} solutions of the complex at room temperature. Molar absorption coefficients are reported in brackets. sh = shouldering peak.

Going from acetonitrile to water led to tremendous change of the visible light absorption of compound **1** which absorbed light at longer wavelengths (up to 580 nm) and more intensely (ε = 34.1*10^3 L.mol^{-1}.cm^{-1} at 493 nm). This strong absorption band at 493 nm was also observed for compound **2** and is typical of the n-π* transition occurring between the phenol and the carbonyl moieties of the fluorescein fragment (OH(p) → π*(C^O)). This transition is no longer observed in acetonitrile, likely due to the major presence of the unconjugated lactone form of fluorescein. These conclusions are based on previous

studies reporting deep investigations over the origin of the various absorption bands occurring in the fluorescein absorption spectra along with their pH dependence. [15, 16]

The pH titration curves displayed in **Figure 3** revealed strong influence of the pH on the visible light absorption properties of complex **1**. A sigmoidal fit of the absorption band enhancement was used to estimate the pKa of the carboxylic acid function of the fluorescein fragments (see **Figure 3**, inset). A pKa of 5.1 ± 0.1 was determined, which indicated a slightly more acidic carboxylic acid function than in free fluorescein (pKa = 5.5 ± 0.1, see SI, Figure S13). This agreed with the electron withdrawing effects of the Schiff base functions and the Ru^{2+} cation coordinated to the ligand. The absorption band at 435 nm appearing at pH 2 is typical of the cationic form of fluorescein, while those at 455 and 477 nm are attributed to its neutral form.[17] As displayed in **Figure 3**, the UV region absorption was weakly affected by pH changes. Interestingly, the shape of the absorption spectrum of the complex in water at pH 4 was similar to the one in acetonitrile in **Figure 2**, which indicated that the fluorescein moiety was in the same ionization state and in similar tautomeric ratios in both conditions. Unsurprisingly, the light absorption spectrum of $[Ru(phen)_3]^{2+}$ was not affected by pH variations, as it does not possess any chemical functionality that could be protonated or deprotonated in aqueous conditions.

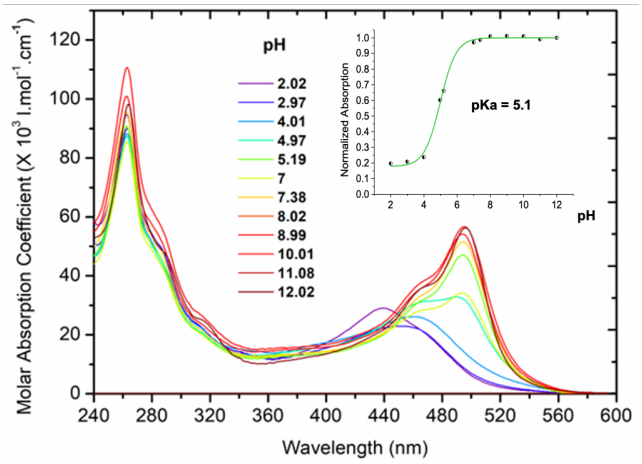

Figure 3. Light absorption spectra of complex **1** in water at various pH. The inset displays the normalized absorption of the complex as function of pH at 490 nm (pH 12.02 as reference) with the corresponding sigmoidal curve fit in green.

Light emission properties of the complexes were also investigated in acetonitrile and in deionized water. Strong and broad photoluminescence were observed for complex **1,** centred at *ca.* 600 nm in acetonitrile with quantum yields, excited-state lifetimes and radiative deactivation rate constants close to those of $[Ru(phen)_3]^{2+}$ (**Table 2**). This indicated a ^{3}MLCT-type emitting state, as already reported for $[Ru(phen)_3]^{2+}$.[18] In deionized water, a much stronger and sharper emission was observed at 515 nm with higher quantum yields (>0.1), shorter excited state lifetimes (4-5 ns) and higher radiative deactivation constants (> 10^6 s^{-1}) close to those of the fluorescein dianion (**Figure 4** and **Table 2**). A very similar behaviour was observed for complex **2**. This highlights the impressive solvent sensitivity of the complex going from a Ru-centred emission in acetonitrile to a fluorescein-centred emission in the protic solvent, water.

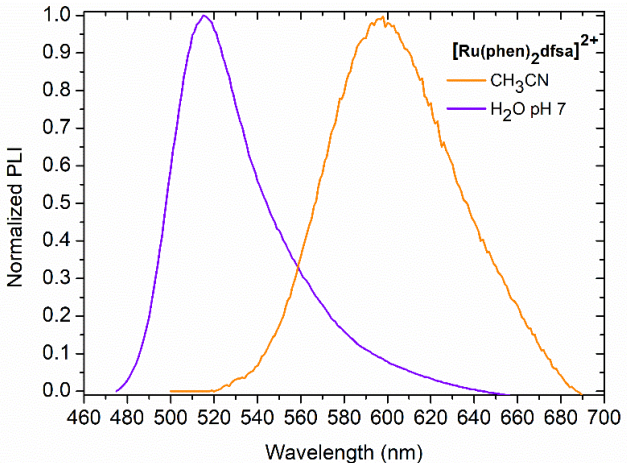

Figure 4. Normalized photoluminescence spectra of $[Ru(phen)_2dfsa]^{2+}$ **1** at a concentration of 5 µM in acetonitrile (orange) and in deionized water (violet) (λ_{exc} = 450 nm) recorded under inert atmosphere.

At this stage, it should be noted that the reported lifetime for **1** and **2** were shorter than 10 ns in deionized water. In fact, the Ru centred emission might be hidden by the intense luminescence of the fluorescein fragment in water. This can be linked to the fact that the fluorescein moiety is present in its poorly emissive neutral form in acetonitrile while its bright anionic form is predominant in deionized neutral water.[15] To shine light on this hypothesis, delay maps, which consist in recording emission spectra of the compounds at different time intervals after excitation, showed that the emission of fluorescein at 515 nm was completely turned off 50 ns after the laser pulse (λ_{exc} = 450 nm). However, photoluminescence from the Ru centre was unambiguously observed at longer time range and was only completely switched off 20-30 µs after the excitation pulse. The excited-state lifetime was well altered upon pH change with the longest lifetime observed at pH 10 (1030 ns) and the shortest one measured at pH 2 (625 ns). The same experiments were carried out for complex **2** and showed a weaker pH effect on the excited-state lifetime of the complex (see SI, Figure S16-S19).

Table 2 - Emission data in CH_3CN and H_2O at 298 K under ambient air for complexes 1-3.

Complex	Emission λ_{max}[a,b][nm]		Φ_{em}[c,d]		τ[c] [ns]		k_r [10^3 s^{-1}]	
	CH_3CN	H_2O	CH_3CN	H_2O	CH_3CN	H_2O	CH_3CN	H_2O
$[Ru(phen)_3]^{2+}$	604	606	0.028	0.072	460	920	60.9	78.0
Fluorescein	599	515	0.004[f]	0.17[f]	6	4	666	$42*10^3$
$[Ru(phen)_2dfsa]^{2+}$ **1**	598	514	0.017[e]	0.11[f]	522	5	32.5	$27*10^3$
$[Ru(phen)_2mfsa]^{2+}$ **2**	599	514	0.018	0.10	488	4	36.9	$25*10^3$
$[Ru(phen)_2salphen]^{2+}$ **3**	599	600	0.018	0.075	688	1222	26.2	61.4

[a] Measurements were made with solutions 5×10^{-6} mol.L^{-1} in complex under air. [b] λ_{exc} = 450 nm. [c] Measurements were made with 5×10^{-6} mol.L^{-1} solutions of the complex under nitrogen. [d] Measurements relative to $[Ru(bpy)_3]^{2+}$ in nitrogen purged aqueous solution (Φ_{em} = 0.063) and in nitrogen purged acetonitrile (Φ_{em} = 0.094); errors are estimated as 5%.[19] [e] The luminescence was observed with $\Phi_{em} < 10^{-5}$. n.d. = not determined. [f] Measurements relative to fluorescein in aqueous solution at pH 10 (Φ_{em} = 0.93); errors are estimated as 5%.[20]

Evaluation of pH effect on the $^1O_2$ photoproduction yields

By virtue of their long-lived excited state, Ru^{II} polypyridyl based PSs can generate $^1O_2$ under visible light irradiation with high yields through energy transfer to molecular oxygen. The $^1O_2$ quantum yield (Φ_Δ) corresponds to the ratio of the number of produced $^1O_2$ molecules to the number of absorbed photons and can be measured by spectroscopic techniques. In the present project, the Φ_Δ were determined in water by monitoring the decomposition of anthracene-9,10-divinylsulfonate (AVS) which reacts efficiently with the photoproduced $^1O_2$ through a [4+2] cycloaddition. Practically, a solution of AVS ($C \approx 10^{-4}$ mol.L^{-1}; $A \approx 1$ at 395 nm) using a catalytic concentration of the Ru^{II} complex ($C \approx 10^{-6}$ mol.L^{-1}; $A \approx 0.025$ at 465 nm) was irradiated at 465 nm. The decomposition of AVS was followed over 15 min, via the decay of its absorption band at 395 nm (**Figure 5**). The decay was much greater at pH 5.5 (**Figure 5A**) than at pH 7 (**Figure 5B**). The insets represent the linear fit of the decay that can be used to determine the $^1O_2$ quantum yield of the complex Φ_Δ (Ru) as explained hereafter. As displayed in **Table 3**, the Φ_Δ of complex **1** is relatively low for a Ru^{II} complex in the pH 7-7.5 region (Φ_Δ = 0.07-0.09) but increased at pH=5.5, reaching a Φ_Δ of 0.66. For the $[Ru(phen)_3]^{2+}$ reference complex, $^1O_2$ quantum yield Φ_Δ = 0.23 was determined in deionized water, which is very close to the values reported for $[Ru(bpy)_3]^{2+}$.[21] In contrast to **1**, the Φ_Δ of $[Ru(phen)_3]^{2+}$ remained unaltered upon decreasing pH, which is consistent for a complex without any protonation sites. Taking fluorescein as the reference (Φ_Δ = 0.030 at pH 7),[22] its Φ_Δ increases steadily with acidity and is doubled when going from pH 7 to pH 5.5. However, the measured Φ_Δ values were weak and did not fully account for the large Φ_Δ increase observed for compound **1**. The same trend of enhanced Φ_Δ with increased acidity was also observed for complexes **2** and **3,** but to a lesser extent than for **1,** suggesting that protonation of both the Schiff base and fluorescein moieties could be involved in the pH activation process.

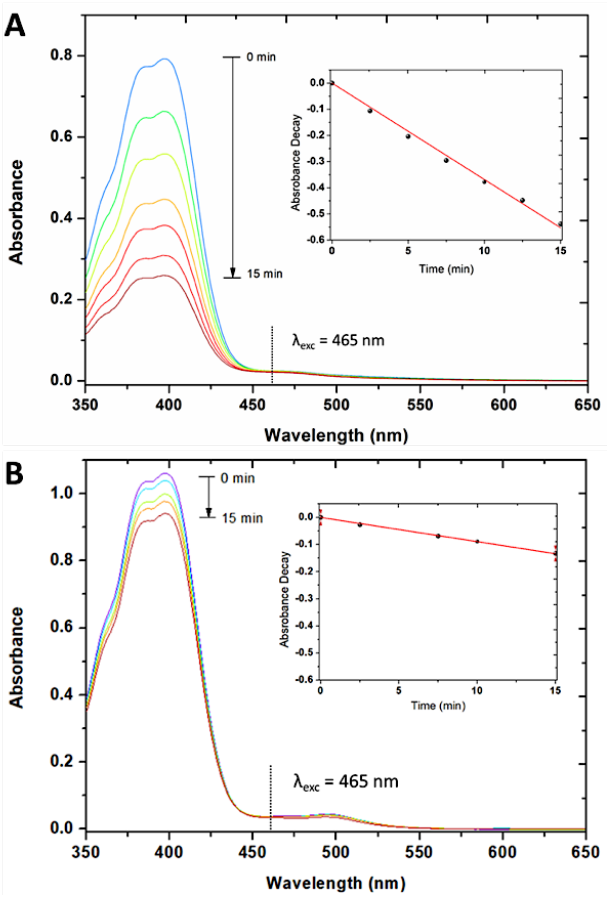

Figure 5 – Absorption spectra monitoring the decomposition of AVS by $^1O_2$ upon 15 minutes of blue light irradiation (465 nm, A = 0.025) of $[Ru(phen)_2dfsa]^{2+}$ **1** at pH 5.5 (A) and at pH 7 (B). The insets show the absorption decays at 395 nm corresponding to the AVS decomposition and were fitted linearly.

Table 3– Measured $^1O_2$ quantum yields at various pH for the studied complexes 1-3 and the reference compounds.

Photosensitizer	logP[a,b]		Φ_Δ[a,c]				
	pH 5.5	pH 7.5	pH 4.5	pH 5.5	pH 6.5	pH 7	pH 7.5
$[Ru(phen)_3]^{2+}$	-1.73	-1.78	0.28	0.24	0.22	0.23	0.23
Fluorescein	-2.83	-3.00	0.080	0.062	0.041	0.030	0.028
$[Ru(phen)_2dfsa]^{2+}$ **1**	-2.02	-2.23	0.71	0.66	0.18	0.09	0.07
$[Ru(phen)_2mfsa]^{2+}$ **2**	-1.89	-2.11	0.46	0.38	0.20	0.11	0.11
$[Ru(phen)_2salphen]^{2+}$ **3**	-1.03	-1.13	0.42	0.30	0.24	0.18	0.16

[a] Measurements were performed on aerated solutions. [b] Partition coefficients between water and octanol, log P = log(C_{oct}/C_{wat}), determined through absorption spectroscopy measurements (experimental error estimated to 10%). [c] The singlet oxygen quantum yield of fluorescein at pH 7 was taken as reference.[22, 23]

Evaluation of the complexes as photosensitizers against cancer cells

As $^1O_2$ photogeneration of the compounds could be modulated by pH, we tested whether these complexes could be candidates for PDT. To this end, U2OS osteosarcoma cells were incubated in the presence of various concentrations of compounds **1** and **3** or the reference compound $[Ru(phen)_3]^{2+}$. Cell viability was then assessed following blue light irradiation (405 nm: 15.7 Wm^{-2}) or without irradiation (dark control). As displayed in **Figure 6**, the PSs exhibit a low dark cytotoxicity with IC_{50} values over 100 µM. However, upon light irradiation, cytotoxicity of the PSs increased by several orders of magnitude. The IC_{50} values after 90 min of incubation followed by 30 min of irradiation was of 14.8 µM for $[Ru(phen)_3]^{2+}$, and lower IC_{50} values of 3.96 and 2.10 µM were found for the Ru^{II} Schiff base complexes **1** and **3**, respectively (Table 4).

Taking advantage of the luminescence of the compounds, a first insight into the cellular penetration potency and subsequent cellular localization of the compounds upon incubation using confocal microscopy imaging was achieved. Cell penetration assays were performed using the same U2OS osteosarcoma cell line and DRAQ5 as nuclear marker. Compounds **1** and **2** penetrated U2OS cells within 90 min and located mainly in the nucleus (see SI, Figure S35), which is consistent with their negative logP values (**Table 3**). Complex **3**, that possesses salicylic moieties instead of fluorescein fragments, also penetrated the cell but localizes both in the nucleus and in the cytosol (see SI, Figure S36). The preferential targeting of complexes **1** and **2** to the nucleus compared to compound **3** might be related to the extended aromatic structure of fluorescein in comparison to salicylic fragments conferring a higher affinity towards the genetic material.

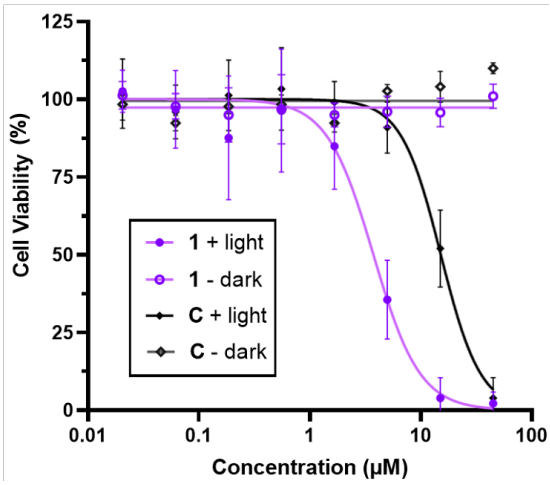

Figure 6 - Cell viability of U2OS cells in full medium (DMEM, pH 7.4) depending on the concentration of complexes **1** (purple) and the control $[Ru(phen)_3]^{2+}$ (**C**) (black) upon blue light irradiation for 30 min (+ light) and in the dark (- dark). Cell viabilities were determined using the tetrazole derivative cell proliferation reagent WST-1 test after a further 24 h of incubation.

Table 4 – Calculated IC_{50} values of the different compounds for given conditions.

Conditions	$[Ru(phen)_3]^{2+}$	1	3
light, full medium	14.8 ± 2.1 µM	3.96 ± 0.65 µM	2.10 ± 0.60 µM
light pH 5.5	14.8 ± 1.9 µM	0.93 ± 0.23 µM	1.15 ± 0.15 µM
light pH 7.5	13.8 ± 2.1 µM	3.84 ± 0.75 µM	1.93 ± 0.27 µM
dark, full medium	> 100 µM	> 100 µM	> 100 µM

dark, pH 5.5	79 ± 20 µM	> 96 µM	> 100 µM
dark, pH 7.5	> 100 µM	> 100 µM	> 100 µM

The results represent mean ± CI of 12 experiments (CI: confidence interval 95%). Irradiation time is of 30 min.

Evaluation of the complexes as pH sensitive photosensitizers

The results obtained in the previous sections demonstrated the applicability of the fluoresceine-containing compounds as PS candidates for PDT. To test their potential as pH-sensitive PDT agents, U2OS cells were incubated for 5 minutes in an "Intracellular pH Calibration Buffer Kit, Thermo Fisher Scientific" (see the experimental section) at pH 5.5 or 7.5 prior to and during the irradiation step. This protocol was recently implemented by Resch-Genger and co-workers for a similar study.[9] These experiments aim to assess the impact of acidity on the photocytotoxicity of the compounds, as cancer cells are often reported to evolve at more acidic pH than healthy cells. The stability of the Schiff base link in complexes **1-3** was assessed at pH 5.5 for a duration of 72 hours, demonstrating no degradation of the compounds. The robust conjugation observed in these Schiff bases is widely acknowledged as a factor contributing to their increased resistance to hydrolysis under mildly acidic conditions. The ability of the salphen site of complex **1** to bind to Mg^{2+} cations was also tested using a physiological concentration of Mg^{2+}. The unchanged UV/vis spectra of complex **1** confirmed that the complex does not bind to Mg^{2+}. The $[Ru(phen)_3]^{2+}$ complex was used as a control as its ability to photoproduce singlet oxygen is not influenced by pH variations. **Table 4** gathers the IC_{50} values obtained in the dark and under irradiation for the different compounds at pH 5.5 and 7.5, as well as in full medium conditions (DMEM, pH 7.4). The toxicity of the compounds in the dark appeared to be very low, with most IC_{50} values above 100 µM, irrespective of the pH. However, upon light irradiation with blue light, cytotoxicities drastically increased giving rise to high photo-indexes. As depicted in **Figure 7** and in agreement with a pH independent photoproduction of $^1O_2$, the control compound $[Ru(phen)_3]^{2+}$ displayed similar cytotoxicity upon irradiation at pH 5.5 and 7.5 with IC_{50} values of 13.2 and 14.2 µM, respectively. Hence, with IC_{50} values close to those measured in full medium conditions (14.8 µM), the impact of the "intracellular pH calibration buffer" incubation step has no deleterious effect on cell viability.

Strikingly, the 4-5-fold decrease of the IC_{50} determined for complex **1** at pH 5.5 compared to pH 7.5 clearly demonstrated that cytotoxic ROS photoproduction was pH-dependent. The IC_{50} decrease was however lower than expected from the $^1O_2$ photoproduction assays performed *in vitro*. We hypothesized that this lower effect might be due to the accumulation of the compounds in various subcellular compartments which might be different upon change of intracellular pH. We therefore repeated cell penetration assays under those pH conditions to evaluate their impact on cellular uptake and localization of the compounds.

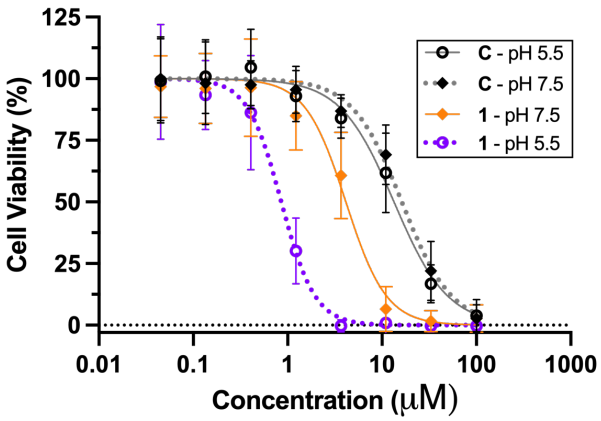

Figure 7 - Cell viability of U2OS cells after a 5 min incubation step and blue light irradiation for 30 min in buffer at pH 5.5 or 7.5 depending on the concentration of complexes **1** (purple and orange) and the control $[Ru(phen)_3]^{2+}$ (**C**) (grey). Cell viabilities were determined using the tetrazole derivative cell proliferation reagent WST-1 test after a further 24 h of incubation.

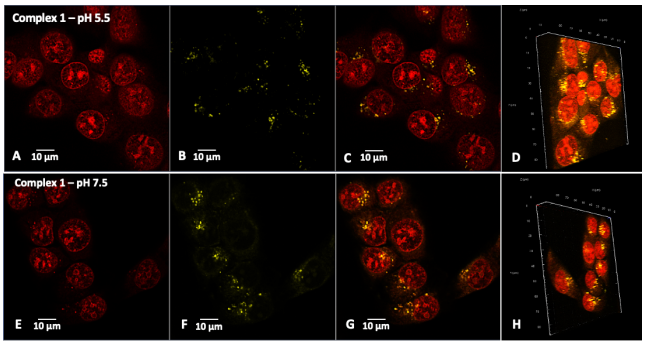

Figure 8 - Cell penetration studies. Confocal microscopy pictures of U2OS cells after incubation with 10 µM of complex **1** in DMEM for 1,5 hours followed by incubation for 5 minutes in a buffer at either pH 5.5 (A-C) or pH 7.5 (E-G). Nucleus was stained in red by DRAQ5 (A and D); the fluorescence of the fluorescein moiety of the Ru^{II} complex appears in yellow (B and F). C and G are merged images. Images D and H show 3D images rebuilt from Z-stack experiments.

Cell penetration assays performed by 2D and 3D confocal microscopy revealed that incubation at pH 5.5 drastically changed the location of complex **1** in the cell, with the compound no longer accumulating in the nucleus, but rather into smaller cell compartments (**Figure 8**, top). Even if the complex did not accumulate in the nucleus in these pH conditions, the lower IC_{50} was consistent with higher photocytotoxicity. The same experiment was repeated using a pH 7.5 buffer (**Figure 8**, bottom) and revealed that complex **1** also accumulated outside the nucleus.

These cell penetrations assays carried out at various pH highlighted the strong sensitivity of the subcellular location of the compounds as a function of the pH. While their dark cytotoxicities are very low (IC_{50} > 100 μM) , the light-induced cytotoxicities in the submicromolar range observed for complex **1** with an internal pH of 5.5 outperform PSs studied in the same conditions against U2OS.[24, 25] However, no comparison of the advantages of the pH-controlled cytotoxicity of the complexes can be made as there are presently no data available for other pH-controlled Ru^{II} complexes able to photosensitize molecular oxygen.

CONCLUSIONS

This research included the synthesis, characterization and photophysical studies of pH-activatable luminescent $^1O_2$-generating Ru^{II} Schiff base complexes. The Ru centre is responsible for the ability of the compound to photoproduce $^1O_2$ with high quantum yields, while the fluorescein moiety and particularly its carboxylic acid function is the origin of the on/off switch of the PS in the pH 5-7 range. Consequently, the resulting complexes show a pH-dependent $^1O_2$ generation ability which make them more effective at the acidity level observed in most tumoral tissues (pH 5.5-6.5). The photophysical properties of the complexes appeared to be strongly influenced by their environment. In acetonitrile, the emission was centred at *ca.* 600 nm with excited-state lifetimes >400 ns, while in water, fluorescence was measured at *ca.* 515 nm with short excited-state lifetimes (4-5 ns). This can be explained by the open form of the fluorescein moiety present in protic solvents, such as water, which lead to a bright emission centred on the fluorescein fragment, likely hiding the Ru-centred emission. In acetonitrile, the poorly emissive lactone form of fluorescein dominates, allowing Ru-centred emission to be seen. This hypothesis was further confirmed by time-resolved emission spectra.

This study also aimed at evaluating the ability of the complexes to act as photosensitizers for PDT. The $^1O_2$ trap experiments showed the pH sensitivity of the $^1O_2$ photoproduction quantum yields in water, which increased by a factor 10 in slightly acidic conditions compared to the physiological conditions of pH 7.5. *In cellulo* studies using U2OS osteosarcoma cell lines showed that light irradiation triggered an increased cytotoxicity of the compounds. Indeed, cells irradiated with blue light for 30 min were almost completely eradicated at micromolar concentrations of the complex, while in dark conditions, concentrations of several orders of magnitude higher were tolerated. Moreover, we showed that the pH control of the photosensitizer, and by extension the $^1O_2$ photoproduction, can provide the basis for pH-dependent photocytotoxicity of Ru^{II} complexes. This was demonstrated with the $[Ru(phen)_2dfsa]^{2+}$ complex (pKa=5.1) that showed a 4-5-fold increase in photocytotoxicity at pH 5.5 compared to pH 7.5, reaching an IC_{50} of 0.88 μM. This 4-5 fold increase is similar to the one reported for pH controllable BODIPY dyes and is more likely related to the "switched-on" $^1O_2$ generation at lower pH.[9] Cell penetration assays revealed a high sensitivity to the intracellular acidity on the cell location of the compounds. The results presented underline the potential application of Ru^{II} Schiff base complexes bearing a pH switchable moiety, such as fluorescein, as pH-controllable $^1O_2$-generating photosensitizers. The compounds also showed higher photo-indexes compared to the previously reported pH-controllable BODIPY dyes. The developed compounds are also more water soluble and easier to prepare than the BODIPY and porphyrin dyes previously studied as pH activatable photosensitizers.[6, 8] Future research will aim at investigating the further potential of the compounds with studies on *in vivo* systems.

EXPERIMENTAL SECTION

Reagents and characterization

$[Ru(phen)_2Cl_2]$ precursor, 5,6-diamino-1,10-phenanthroline and 5-amino-1,10-phenanthroline were synthesized according to previously described literature protocols.[25] All solvents and reagents for the synthesis were of reagent grade and were used without any further purification. All solvents for the spectroscopic and electrochemical measurements were of spectroscopic grade. Water was purified with a Millipore Milli-Q system. ^1H NMR experiments were performed in CD_3CN or d6-DMSO on a Bruker AC-300 Avance II (300 MHz) or on a Bruker AM-500 (500 MHz) at 20 °C. The chemical shifts (given in ppm) were measured vs the residual peak of the solvent as the internal standard. High-resolution mass spectrometry (HRMS) spectra were recorded on a Q-Exactive orbitrap from ThermoFisher using reserpine as the internal standard. Samples were ionized by electrospray ionization (ESI; capillary temperature = 320 °C, vaporizer temperature = 320 °C, sheath gas flow rate = 5 mL min^{-1}). HPLC analyses were performed on a Waters Alliance 2690 using a XBridge C18 column (50 x 4.6 mm; 2.5 μm) as stationary phase. The elutions were performed with a gradient starting from water/acetonitrile 90-10 (0.1% TFA) to water/acetonitrile 10-90 (0.1% TFA).. All compounds are >95% pure by HPLC analysis.

Synthesis

dfsa ligand. To a refluxing solution of 5,6-diamino-1,10-phenanthroline (105 mg, 0.50 mmol) in ethanol were added two equivalents of fluorescein-5-carbaldehyde (360 mg, 1.00 mmol) and a catalytic amount of acetic acid (20 μL). The reaction was maintained at reflux for 3 hours. The so-formed orange precipitate was filtered and succinctly washed with ethanol and ether which afforded the dfsa ligand (135 mg, 0.15 mmol, 31%) as an orange solid. **^1H NMR (DMSO-d_6, 300 MHz)** δ 12.37 (2H, s, -COO***H***), 10.24 (2H, s, -O***H***), 9.72 (2H, s, -*CH*N-), 9.41 (2H, dd, J = 8.2, 1.5 Hz, ***H*$_{12}$**), 9.22 (2H, dd, J = 4.7, 1.5 Hz, ***H*$_{10}$**), 8.17 (2H, dd, J = 8.2, 4.7 Hz ***H*$_{11}$**), 8.11 – 8.00 (2 H, m, ***H*$_1$**), 7.93 – 7.68 (4H, m, ***H*$_{2-3}$**), 7.43 – 7.31 (2H, m, ***H*$_4$**), 6.99 (2H, d, J = 1.8 Hz, ***H*$_9$**), 6.90 (2H, d, J = 8.8Hz, ***H*$_6$**), 6.87 – 6.78 (4H, m, ***H*$_{5-8}$**), 6.73 – 6.55 (2H, m, ***H*$_7$**). **HRMS-ESI** calculated for $[C_{33}H_{19}N_4O_5]^+$ fragment: *m/z* 551.13500, found: *m/z* 551.13561.

mfsa ligand. To a refluxing solution of 5-amino-1,10-phenanthroline (195 mg, 1.00 mmol) in ethanol were added fluorescein-5-carbaldehyde (360 mg, 1.00 mmol) and a catalytic amount of acetic acid (20 μL). The reaction was maintained at

reflux for 3 hours. The so-formed salmon precipitate was filtered and succinctly washed with ethanol and ether which afforded the mfsa ligand (223 mg, 0.42 mmol, 42%) as an orange solid. **^{1}H NMR (DMSO-d$_6$, 300 MHz)** δ 10.22 (broad s, 1H, -O***H***), 9.73 (s, 1H, -C***H***N), 9.20 (dd, *J* = 4.2, 1.7 Hz, 1H, ***H$_{13}$***), 9.11 (dd, *J* = 4.3, 1.7 Hz, 1H, ***H$_{14}$***), 8.65 (dd, *J* = 8.3, 1.7 Hz, 1H, ***H$_{11}$***), 8.58 (dd, *J* = 8.2, 1.8 Hz, 1H, ***H$_{16}$***), 8.08 (s, 1H, ***H$_{10}$***), 8.04 (d, *J* = 7.7 Hz, 1H, ***H$_1$***), 7.89 (dd, *J* = 8.3, 4.2 Hz, 1H, ***H$_{12}$***), 7.88 – 7.80 (m, 2H, ***H$_3$*** and ***H$_{15}$***), 7.79 – 7.72 (m, 1H, ***H$_2$***), 7.35 (d, *J* = 7.7 Hz, 1H, ***H$_4$***), 6.94 (s, 1H, m, ***H$_5$***), 6.90 (d, *J* = 8.9 Hz, 1H, ***H$_9$***), 6.82 (d, *J* = 8.9 Hz, 1H, ***H$_8$***), 6.63 (d, *J* = 1.0 Hz, 2H, ***H$_6$*** and ***H$_7$***). **HRMS-ESI** calculated for $[C_{33}H_{19}N_3O_5]^+$: *m/z* 536.12410, found: *m/z* 536.12580.

General procedure for the chelation of [Ru(phen)$_2$Cl$_2$]. The dichloro precursor $[Ru(phen)_2Cl_2]$ (1.0 eq) and the ligand (1.0 eq) were mixed in absolute ethanol. The reaction medium was then stirred at 80 °C until the precursor was consumed as monitored by TLC. Afterwards, ethanol was evaporated and addition of small portions of an aqueous solution of NH_4PF_6 yielded to the formation of a precipitate. After centrifugation, the crude solid was washed several times with water and was then dried under reduced pressure. The residue was finally purified by flash chromatography on silica gel (CH_3CN/H_2O/ KNO_{3sat}). The addition of a saturated solution of KNO_3 to the eluent mixture allows to increase the ionic strength of the eluent and eases complexes purification. The counter-anion exchange from PF_6 to Cl was performed by adding small portions of NBu_4Cl to a solution of the complex in acetone. This led to the precipitation of the complex which was then washed three times with acetone to remove any exceeding salts.

[Ru(phen)$_2$dfsa]$^{2+}$ 1. Using general procedure with $[Ru(phen)_2Cl_2]$ (20 mg, 0.038 mmol) and dfsa ligand (33 mg, 0.038 mmol) gave the crude product that was purified by flash chromatography on silica (CH_3CN/H_2O/ KNO_{3sat} 10:1:1/2) to provide $[Ru(phen)_2dfsa]^{2+}$ as a red solid (32 mg, 0.020 mmol, 52%). **R$_f$** 0.28 (CH_3CN/H_2O/ KNO_{3sat} 10:1:1/2); **^{1}H NMR (CD$_3$CN, 500 MHz)** δ 13.55 (s, 1H, -***COOH***), 9.08 (d, *J* = 8.1 Hz, 2H, ***H$_c$***), 8.53 (d, *J* = 1.3 Hz, 2H, ***H$_2$***), 8.51 (d, *J* = 1.2 Hz, 2H, ***H$_9$***), 8.18 (s, 4H, ***H$_5$*** and ***H$_6$***), 8.02 (broad s, 2H, ***H$_d$***), 7.87-7.93 (m, 6H, ***H$_a$***, ***H$_4$*** and ***H$_7$***), 7.87 (m, 2H, ***H$_k$***), 7.71 (dd, *J* = 7.4, 1.4 Hz, 2H, ***H$_b$***), 7.67 (dd, *J* = 7.3 Hz, 4.6 Hz, 2H, ***H$_i$***), 7.55 (m, 6H, ***H$_g$***, ***H$_3$*** and ***H$_8$***), 7.23 (m, 2H, ***H$_j$***), 7.20 (d, *J* = 7.5 Hz, 2H, ***H$_l$***), 6.80 (d, *J* = 1.6 Hz, 2H, ***H$_e$***), 6.69 – 6.64 (m, 2H, ***H$_f$***), 6.64 – 6.58 (m, 2H, ***H$_m$***). **HRMS-ESI** calculated for $[C_{57}H_{34}N_8O_5Ru]^{2+}$*: m/z* 506.08492, found: *m/z* 506.08423.

[Ru(phen)$_2$mfsa]$^{2+}$ 2. Using general procedure with $[Ru(phen)_2Cl_2]$ (20 mg, 0.038 mmol) and mfsa ligand (20 mg, 0.038 mmol) gave the crude product that was purified by flash chromatography on silica (CH_3CN/H_2O/ KNO_{3sat} 10:1:1/2) to provide $[Ru(phen)_2mfsa]^{2+}$ as an orange solid (28 mg, 0.023 mmol, 60%). **R$_f$** 0.31 (CH_3CN/H_2O/ KNO_{3sat} 10:1:1/2); **^{1}H NMR (DMSO-d6, 500 MHz)** δ 8.88 (dd, *J* = 8.5, 1.2 Hz, 2H), 8.78 (d, *J* = 1.3 Hz, 2H), 8.76 (d, *J* = 1.3 Hz, 2H), 8.76 – 8.73 (m, 2H), 8.38 (s, 4H), 8.38 (s, 1H), 8.29 (dd, *J* = 8.5, 1.2 Hz, 2H), 8.10 – 8.03 (m, 7H), 8.00 (dd, *J* = 5.2, 1.2 Hz, 2H), 7.83 – 7.76 (m, 5H), 7.76 – 7.75 (m, 1H), 7.74 – 7.73 (m, 1H), 7.69 (dd, *J* = 8.5, 5.3 Hz, 2H), 7.56 (dd, *J* = 5.1, 1.2 Hz, 2H), 7.45 (dd, *J* = 8.4, 5.1 Hz, 2H), 7.08 (s, 2H), 6.93 (s, 2H).

Photophysical measurements

UV/Vis absorption spectra were recorded on a Shimadzu UV-1700 spectrophotometer. Room temperature luminescence spectra were recorded on a Varian Cary Eclipse instrument. Quantum yields were obtained using $[Ru(bpy)_3]^{2+}$ as a reference.[19] Luminescence lifetime measurements were performed after irradiation at λ=450 nm obtained as the second harmonic of a titanium: sapphire laser (picosecond Tsunami laser Spectra at a repetition rate of 80 kHz. A Fluotime 200 instrument from AMS Technologies was used for the decay acquisition. It consists of a GaAs microchannel plate photomultiplier tube (Hamamatsu model R3809U-50) followed by a time-correlated single-photon counting system from Picoquant (PicoHarp300). The ultimate time resolution of the system is close to 4 ps. Luminescence decays were analyzed with FLUOFIT software available from Picoquant. Steady state luminescence titrations were performed in 10 mM HEPES pH 7.4, 50 mM NaCl and 100 mM KCl. The complex concentration was kept at 5 µM. For delay maps, a Xenon lamp was used to generate visible range light and near-UV light. Emission spectra were recorded thanks to the Hamamatsu 928 PMT-LP phototube. The excitation source was a laser of 420 nm wavelengths. All the measurements were done with 30 scans and were integrated over time (0 ns to 30 µs). All the data were transferred onto a PC and were reworked using Origin.

Singlet oxygen quantum yield

Singlet oxygen quantum yields of the complexes were determined in milliQ water by monitoring the decomposition of AVS (= Anthracene-9,10-divinylsulfonate), a $^1O_2$ trap, on a time range extending from 0 to 15 minutes. Practically, a solution containing AVS (Absorbance = 1 at 395 nm) and the photosensitizer (Absorbance = 0.025-0.05 at 465 nm was irradiated at 465 nm using a LED (465 nm). The decomposition of AVS was then monitored by analysing the absorption decay of AVS at 395 nm by a UV-1700 Pharma Spec Shimadzu. The Φ_Δ of the complex (Ru) can be obtained by comparing the measured slope of AVS decomposition k(Ru) with the one measured for the reference compound fluorescein k(fluo) whose the Φ_Δ is reported ($\Phi_\Delta = 0.030$).[23] The Φ_Δ of the Ru complex is then obtained after correction of the absorbance at 465 nm (A_{465}) using the following **Equation ES1**:

$$\Phi\Delta\,(\mathrm{Ru}) = \Phi\Delta\,(\mathrm{fluo})\,\frac{\mathrm{A}\,(\mathrm{fluo})\,k(Ru)}{A\,(Ru)\,k(fluo)}$$

Equation ES1

Cell penetrations assays

U2OS cells were grown at 37 °C in a humidified atmosphere with 5% CO_2 in DMEM medium (Westburg) containing 10% fetal bovine serum (FBS) (Gibco) and 1% penicillin/streptomycin (Westburg). 20000 cells were seeded onto a coated microscope slide and incubated with 20 µM of complex for 1,5 h in the dark. After incubation, the medium containing the complex was removed, and fresh medium was added to the cells. The cells were rinsed in pre-warmed PBS, fixed in 4% paraformaldehyde (VWR) for 10 min, and labelled with DRAQ5 (eBioscience) following the instructions of the manufacturer. A confocal laser scanning microscopy system (Zeiss LSM 710) was used to acquire the images, which were processed with Zen software.

Cell penetrations assays at various pH

U2OS cells were grown at 37 °C in a humidified atmosphere with 5% CO_2 in DMEM medium (Westburg) containing 10%

fetal bovine serum (FBS) (Gibco) and 1% penicillin/streptomycin (Westburg). 20000 cells were seeded onto a coated microscope slide and incubated with 20 µM of complex for 1,5 h in the dark. After incubation, the medium containing the complex was removed, and the cells were incubated for 5 minutes with a buffer solution at either pH 5.5 or pH 7.5 containing nigericin and valinomycin antibiotics (the intracellular pH calibration buffer kit was purchased from ThermoFisher). The cells were then rinsed in pre-warmed PBS, fixed in 4% paraformaldehyde (VWR) for 10 min, and labelled with DRAQ5 (eBioscience) following the instructions of the manufacturer. A confocal laser scanning microscopy system (Zeiss LSM 710) was used to acquire the images, which were processed with Zen software.

Photo-cytotoxicity experiments

U2OS cells were cultured for 24 h in DMEM (Westburg) containing 10% FBS (Gibco) and 1% penicillin/streptomycin (Westburg) in 96-well plates at an initial density of 10000 cells/well. The supernatant was then removed and fresh medium containing different concentrations the complex was added. After one hour and a half of incubation at 37 °C in the dark, cells were rinsed twice with 1x PBS to remove non-internalized complex. They were then illuminated for 30 min with blue LEDs (LED strip IP68 60 $LEDm^{-1}$ from Prolumia, 405 nm at 15.7 Wm^{-2}). The distance between the light source and the culture plate was 10 cm. Dark controls were protected from illumination with aluminium foil. Illuminated and control cultures were directly put back in the incubator after addition of fresh medium and incubated for another 24 hours. Cell viability was measured 1-day post-irradiation using 10 µL/well of WST-1 reagent (Roche) following the manufacturer's instructions. The ratio of the optical density at $\lambda = 450$ nm under each set of conditions to that of control cells (non-transfected and non-irradiated, 100% viability) was used to determine the relative viability. Experiments were performed as biological triplicate with 4 measurements each time.

Photo-cytotoxicity experiments at various pH

U2OS cells were cultured for 24 h in DMEM (Westburg) containing 10% FBS (Gibco) and 1% penicillin/streptomycin (Westburg) in 96-well plates at an initial density of 10000 cells/well. The supernatant was then removed and fresh medium containing different concentrations of the complex was added. After one hour and a half of incubation at 37 °C in the dark, cells were rinsed twice with 1x PBS to remove non-internalized complex. Cells were then incubated for 5 minutes with a buffer solution at either pH 5.5 or pH 7.5 containing nigericin and valinomycin antibiotics (the intracellular pH calibration buffer kit was purchased from ThermoFisher) as already reported for this type of study.[6] They were then directly illuminated in the buffer for 30 min with blue LEDs (LED strip IP68 60 $LEDm^{-1}$ from Prolumia, 405 nm at 15.7 Wm^{-2}). The distance between the light source and the culture plate was 10 cm. Dark controls were protected from illumination with aluminum foil. Illuminated and control cultures were directly put back in the incubator after addition of fresh medium and incubated for another 24 hours. Cell viability was measured 1-day post-irradiation using 10 µL/well of WST-1 reagent (Roche) following the manufacturer's instructions. The ratio of the optical density at $\lambda = 450$ nm under each set of conditions to that of control cells (non-transfected and non-irradiated, 100% viability) was used to determine the relative viability. Experiments were performed as biological triplicate with 4 measurements each time.

ASSOCIATED CONTENT

Supporting Information

Description of the synthesis and characterization of the compounds; ^{1}H NMR spectra of new compounds; HRMS spectra of new compounds; figures of UV/Vis pH titrations; delay maps data; singlet oxygen quantum yields measurements; figures of cell viabilities and cell penetration assays; HPLC analysis (PDF).

The Supporting Information is available free of charge on the ACS Publications website.

AUTHOR INFORMATION

Corresponding Author

*Benjamin.Elias@uclouvain.be

Notes

The authors declare no conflict of interest.

ACKNOWLEDGMENT

M. G., L.T.-G. and B. E. gratefully acknowledge the Université catholique de Louvain (UCLouvain) and the F.R.S-FNRS (Grant Number U.N021.21) for financial support. L. T.-G. is a chercheur qualifié of the Fonds de la Recherche Scientifique – FNRS. We thank Manon Mahieu and Dr. Gabriel Le Berre for their scientific and technical support.

ABBREVIATIONS

AVS, anthracene-9,10-divinylsulfonate; BODIPY, boron-dipyrromethene; CH_3CN, acetonitrile; dfsa, 5,6-difluoresceindiimine-1,10-phenanthroline; IC_{50}, half-maximal inhibitory concentration; mfsa, 5-monofluoresceindiimine-1,10-phenanthroline; MLCT, metal to ligand charge transfer; PDT, photodynamic therapy; phAMP's, pH-Activated Metallo Prodrugs; PS, photosensitizer; Φ_Δ, quantum yields for singlet oxygen photoproduction; τ, luminescence lifetime.

REFERENCES

(1) Agostinis, P.; Berg, K.; Cengel, K. A.; Foster, T. H.; Girotti, A. W.; Gollnick, S. O.; Hahn, S. M.; Hamblin, M. R.; Juzeniene, A.; Kessel, D.; et al. Photodynamic therapy of cancer: an update. *CA Cancer J. Clin.* **2011**, *61* (4), 250-281. DOI: 10.3322/caac.20114 From NLM. Ishizuka, M.; Abe, F.; Sano, Y.; Takahashi, K.; Inoue, K.; Nakajima, M.; Kohda, T.; Komatsu, N.; Ogura, S.-i.; Tanaka, T. Novel development of 5-aminolevurinic acid (ALA) in cancer diagnoses and therapy. *Int. Immunopharmacol.* **2011**, *11* (3), 358-365. DOI: https://doi.org/10.1016/j.intimp.2010.11.029. Allison, R. R.; Sibata, C. H. Oncologic photodynamic therapy photosensitizers: A clinical review. *Photodiagnosis Photodyn. Ther.* **2010**, *7* (2), 61-75. DOI: https://doi.org/10.1016/j.pdpdt.2010.02.001. Hong, E. J.; Choi, D. G.; Shim, M. S. Targeted and effective photodynamic therapy for cancer using functionalized nanomaterials. *Acta pharmaceutica Sinica. B* **2016**, *6* (4), 297-307. DOI: 10.1016/j.apsb.2016.01.007 PubMed.

(2) Pham, T. C.; Nguyen, V.-N.; Choi, Y.; Lee, S.; Yoon, J. Recent Strategies to Develop Innovative Photosensitizers for Enhanced Photodynamic Therapy. *Chem. Rev.* **2021**, *121* (21), 13454-13619. DOI: 10.1021/acs.chemrev.1c00381.

(3) Klaus, T.; Deshmukh, S. pH-responsive antibodies for therapeutic applications. *J. Biomed. Sci.* **2021**, *28* (1), 11. DOI: 10.1186/s12929-021-00709-7. Li, Z.; Huang, J.; Wu, J. pH-Sensitive nanogels for drug delivery in cancer therapy. *Biomater. Sci.* **2021**, *9* (3), 574-589, 10.1039/D0BM01729A. DOI: 10.1039/D0BM01729A. Hamaguchi, R.; Narui, R.; Wada, H. Effects of Alkalization Therapy on Chemotherapy Outcomes in Metastatic or Recurrent Pancreatic Cancer. *Anticancer Res.* **2020**, *40* (2), 873-880. DOI: 10.21873/anticanres.14020. Morarasu, S.; Morarasu, B. C.; Ghiarasim, R.; Coroaba, A.; Tiron, C.; Iliescu, R.; Dimofte, G.-M. Targeted Cancer Therapy via pH-Functionalized Nanoparticles: A Scoping Review of Methods and Outcomes. *Gels* **2022**, *8* (4), 232.

(4) Gerweck, L. E.; Seetharaman, K. Cellular pH gradient in tumor versus normal tissue: potential exploitation for the treatment of cancer. *Cancer Res.* **1996**, *56* (6), 1194-1198. From NLM. Bogdanov A, B. A.; Chubenko V, V. N., Moiseenko F; V, a. M. Tumor acidity: From hallmark of
cancer to target of treatment. *Front. Oncol.* **2022**, *12*, 979154. Ward, C.; Meehan, J.; Gray, M. E.; Murray, A. F.; Argyle, D. J.; Kunkler, I. H.; Langdon, S. P. The impact

of tumour pH on cancer progression: strategies for clinical intervention. *Explor Target Antitumor Ther* **2020**, *1* (2), 71-100. DOI: 10.37349/etat.2020.00005 From NLM.
Webb, B. A.; Chimenti, M.; Jacobson, M. P.; Barber, D. L. Dysregulated pH: a perfect storm for cancer progression. *Nat. Rev. Cancer* **2011**, *11* (9), 671-677. DOI: 10.1038/nrc3110.
(5) Pinto, A.; Marangon, I.; Méreaux, J.; Nicolás-Boluda, A.; Lavieu, G.; Wilhelm, C.; Sarda-Mantel, L.; Silva, A. K. A.; Pocard, M.; Gazeau, F. Immune Reprogramming Precision Photodynamic Therapy of Peritoneal Metastasis by Scalable Stem-Cell-Derived Extracellular Vesicles. *ACS Nano* **2021**, *15* (2), 3251-3263. DOI: 10.1021/acsnano.0c09938.
(6) Radunz, S.; Wedepohl, S.; Röhr, M.; Calderón, M.; Tschiche, H. R.; Resch-Genger, U. pH-Activatable Singlet Oxygen-Generating Boron-dipyrromethenes (BODIPYs) for Photodynamic Therapy and Bioimaging. *Journal of Medicinal Chemistry* **2020**, *63* (4), 1699-1708. DOI: 10.1021/acs.jmedchem.9b01873.
(7) Hirakawa, K.; Onishi, Y.; Ouyang, D.; Horiuchi, H.; Okazaki, S. pH-Dependent photodynamic activity of bis(6-methyl-3-pyridylmethoxy)P(V)tetrakis(p-methoxyphenyl)porphyrin. *Chem. Phys. Lett.* **2020**, *746*, 137315. DOI: https://doi.org/10.1016/j.cplett.2020.137315. Horiuchi, H.; Kuribara, R.; Hirabara, A.; Okutsu, T. pH-Response Optimization of Amino-Substituted Tetraphenylporphyrin Derivatives as pH-Activatable Photosensitizers. *The Journal of Physical Chemistry A* **2016**, *120* (28), 5554-5561. DOI: 10.1021/acs.jpca.6b05019. Tian, J.; Zhou, J.; Shen, Z.; Ding, L.; Yu, J.-S.; Ju, H. A pH-activatable and aniline-substituted photosensitizer for near-infrared cancer theranostics. *Chemical Science* **2015**, *6* (10), 5969-5977, 10.1039/C5SC01721A. DOI: 10.1039/C5SC01721A.
(8) Horiuchi, H.; Tajima, K.; Okutsu, T. Triply pH-activatable porphyrin as a candidate photosensitizer for near-infrared photodynamic therapy and diagnosis. *J. Photochem. Photobiol. A: Chem.* **2020**, *403*, 112846. DOI: https://doi.org/10.1016/j.jphotochem.2020.112846. Horiuchi, H.; Isogai, M.; Hirakawa, K.; Okutsu, T. Improvement of the ON/OFF Switching Performance of a pH-Activatable Porphyrin Derivative by the Introduction of Phosphorus(V). *ChemPhotoChem* **2019**, *3* (3), 138-144. DOI: https://doi.org/10.1002/cptc.201800248.
(9) Radunz, S.; Wedepohl, S.; Röhr, M.; Calderón, M.; Tschiche, H. R.; Resch-Genger, U. pH-Activatable Singlet Oxygen-Generating Boron-dipyrromethenes (BODIPYs) for Photodynamic Therapy and Bioimaging. *J. Med. Chem.* **2020**, *63* (4), 1699-1708. DOI: 10.1021/acs.jmedchem.9b01873.
(10) Gillard, M.; Bonnet, H.; Lartia, R.; Yacoub, H.; Dejeu, J.; Defrancq, E.; Elias, B. Luminescent Ruthenium(II) Complexes Used for the Detection of 8-Oxoguanine in the Human Telomeric Sequence. *Bioconj. Chem.* **2023**, *34* (2), 414-421. DOI: 10.1021/acs.bioconjchem.2c00578. Weynand, J.; Episkopou, H.; Le Berre, G.; Gillard, M.; Dejeu, J.; Decottignies, A.; Defrancq, E.; Elias, B. Photo-induced telomeric DNA damage in human cancer cells. *RSC Chem. Biol.* **2022**, *3* (12), 1375-1379, 10.1039/D2CB00192F. DOI: 10.1039/D2CB00192F. Gillard, M.; Laramée-Milette, B.; Deraedt, Q.; Hanan, G. S.; Loiseau, F.; Dejeu, J.; Defrancq, E.; Elias, B.; Marcélis, L. Photodetection of DNA mismatches by dissymmetric Ru(ii) acridine based complexes. *Inorg. Chem. Front.* **2019**, *6* (9), 2260-2270, 10.1039/C9QI00133F. DOI: 10.1039/C9QI00133F. Gillard, M.; Piraux, G.; Daenen, M.; Abraham, M.; Troian-Gautier, L.; Bar, L.; Bonnet, H.; Loiseau, F.; Jamet, H.; Dejeu, J.; et al. Photo-Oxidizing Ruthenium(II) Complexes with Enhanced Visible-Light Absorption and G-quadruplex DNA Binding Abilities. *Chem. Eur. J.* **2022**, *28* (66), e202202251. DOI: https://doi.org/10.1002/chem.202202251. Notaro, A.; Frei, A.; Rubbiani, R.; Jakubaszek, M.; Basu, U.; Koch, S.; Mari, C.; Dotou, M.; Blacque, O.; Gouyon, J.; et al. Ruthenium(II) Complex Containing a Redox-Active Semiquinonate Ligand as a Potential Chemotherapeutic Agent: From Synthesis to In Vivo Studies. *J. Med. Chem.* **2020**, *63* (10), 5568-5584. DOI: 10.1021/acs.jmedchem.0c00431. Howerton, B. S.; Heidary, D. K.; Glazer, E. C. Strained Ruthenium Complexes Are Potent Light-Activated Anticancer Agents. *Journal of the American Chemical Society* **2012**, *134* (20), 8324-8327. DOI: 10.1021/ja3009677. Ryan, R. T.; Stevens, K. C.; Calabro, R.; Parkin, S.; Mahmoud, J.; Kim, D. Y.; Heidary, D. K.; Glazer, E. C.; Selegue, J. P. Bis-tridentate N-Heterocyclic Carbene Ru(II) Complexes are Promising New Agents for Photodynamic Therapy. *Inorg. Chem.* **2020**, *59* (13), 8882-8892. DOI: 10.1021/acs.inorgchem.0c00686. Mitchell, R. J.; Gowda, A. S.; Olivelli, A. G.; Huckaba, A. J.; Parkin, S.; Unrine, J. M.; Oza, V.; Blackburn, J. S.; Ladipo, F.; Heidary, D. K.; et al. Triarylphosphine-Coordinated Bipyridyl Ru(II) Complexes Induce Mitochondrial Dysfunction. *Inorg. Chem.* **2023**, *62* (28), 10940-10954. DOI: 10.1021/acs.inorgchem.3c00736. Keane, P. M.; O'Sullivan, K.; Poynton, F. E.; Poulsen, B. C.; Sazanovich, I. V.; Towrie, M.; Cardin, C. J.; Sun, X.-Z.; George, M. W.; Gunnlaugsson, T.; et al. Understanding the factors controlling the photo-oxidation of natural DNA by enantiomerically pure intercalating ruthenium polypyridyl complexes through TA/TRIR studies with polydeoxynucleotides and mixed sequence oligodeoxynucleotides. *Chemical Science* **2020**, *11* (32), 8600-8609, 10.1039/D0SC02413A. DOI: 10.1039/D0SC02413A. Poynton, F. E.; Bright, S. A.; Blasco, S.; Williams, D. C.; Kelly, J. M.; Gunnlaugsson, T. The development of ruthenium(ii) polypyridyl complexes and conjugates for in vitro cellular and in vivo applications. *Chem. Soc. Rev.* **2017**, *46* (24), 7706-7756. DOI: 10.1039/c7cs00680b From NLM. Elmes, R. B. P.; Ryan, G. J.; Erby, M. L.; Frimannsson, D. O.; Kitchen, J. A.; Lawler, M.; Williams, D. C.; Quinn, S. J.; Gunnlaugsson, T. Synthesis, Characterization, and Biological Profiling of Ruthenium(II)-Based 4-Nitro- and 4-Amino-1,8-naphthalimide Conjugates. *Inorg. Chem.* **2020**, *59* (15), 10874-10893. DOI: 10.1021/acs.inorgchem.0c01395.
(11) Heinemann, F.; Karges, J.; Gasser, G. Critical Overview of the Use of Ru(II) Polypyridyl Complexes as Photosensitizers in One-Photon and Two-Photon Photodynamic Therapy. *Acc. Chem. Res.* **2017**, *50* (11), 2727-2736. DOI: 10.1021/acs.accounts.7b00180. Wu, Y.; Li, S.; Chen, Y.; He, W.; Guo, Z. Recent advances in noble metal complex based photodynamic therapy. *Chem. Sci.* **2022**, *13* (18), 5085-5106, 10.1039/D1SC05478C. DOI: 10.1039/D1SC05478C. Frei, A.; Rubbiani, R.; Tubafard, S.; Blacque, O.; Anstaett, P.; Felgenträger, A.; Maisch, T.; Spiccia, L.; Gasser, G. Synthesis, Characterization, and Biological Evaluation of New Ru(II) Polypyridyl Photosensitizers for Photodynamic Therapy. *J. Med. Chem.* **2014**, *57* (17), 7280-7292. DOI: 10.1021/jm500566f.
(12) Qu, F.; Park, S.; Martinez, K.; Gray, J. L.; Thowfeik, F. S.; Lundeen, J. A.; Kuhn, A. E.; Charboneau, D. J.; Gerlach, D. L.; Lockart, M. M.; et al. Ruthenium Complexes are pH-Activated Metallo Prodrugs (pHAMPs) with Light-Triggered Selective Toxicity Toward Cancer Cells. *Inorg. Chem.* **2017**, *56* (13), 7519-7532. DOI: 10.1021/acs.inorgchem.7b01065.
(13) Srivastava, P.; Tavernaro, I.; Genger, C.; Welker, P.; Hübner, O.; Resch-Genger, U. Multicolor Polystyrene Nanosensors for the Monitoring of Acidic, Neutral, and Basic pH Values and Cellular Uptake Studies. *Anal. Chem.* **2022**, *94* (27), 9656-9664. DOI: 10.1021/acs.analchem.2c00944.
(14) Wang, W.; Rusin, O.; Xu, X.; Kim, K. K.; Escobedo, J. O.; Fakayode, S. O.; Fletcher, K. A.; Lowry, M.; Schowalter, C. M.; Lawrence, C. M.; et al. Detection of Homocysteine and Cysteine. *J. Am. Chem. Soc.* **2005**, *127* (45), 15949-15958. DOI: 10.1021/ja054962n.
(15) Klonis, N.; Sawyer, W. H. Spectral properties of the prototropic forms of fluorescein in aqueous solution. *Journal of Fluorescence* **1996**, *6* (3), 147-157. DOI: 10.1007/BF00732054.
(16) Slyusareva, E. A.; Gerasimova, M. A. pH-Dependence of the Absorption and Fluorescent Properties of Fluorone Dyes in Aqueous Solutions. *Russian Physics Journal* **2014**, *56* (12), 1370-1377. DOI: 10.1007/s11182-014-0188-8.
(17) Erbas-Cakmak, S.; Kolemen, S.; Sedgwick, A. C.; Gunnlaugsson, T.; James, T. D.; Yoon, J.; Akkaya, E. U. Molecular logic gates: the past, present and future. *Chem. Soc. Rev.* **2018**, *47* (7), 2228-2248, 10.1039/C7CS00491E. DOI: 10.1039/C7CS00491E.
(18) Boisdenghien, A.; Moucheron, C.; Kirsch-De Mesmaeker, A. [Ru(phen)2(PHEHAT)]2+ and [Ru(phen)2(HATPHE)]2+: Two Ruthenium(II) Complexes with the Same Ligands but Different Photophysics and Spectroelectrochemistry. *Inorg. Chem.* **2005**, *44* (21), 7678-7685. DOI: 10.1021/ic051306f.
(19) Brouwer, A. M. Standards for photoluminescence quantum yield measurements in solution (IUPAC Technical Report). *Pure and Applied Chemistry* **2011**, *83* (12), 2213-2228.
(20) Martin, M. M.; Lindqvist, L. The pH dependence of fluorescein fluorescence. *J. Lumin.* **1975**, *10* (6), 381-390. DOI: https://doi.org/10.1016/0022-2313(75)90003-4.
(21) Wilkinson, F.; Helman, W. P.; Ross, A. B. Quantum Yields for the Photosensitized Formation of the Lowest Electronically Excited Singlet State of Molecular Oxygen in Solution. *J. Phys. Chem. Ref. Data* **1993**, *22* (1), 113-262. DOI: 10.1063/1.555934.
(22) Gandin, E.; Lion, Y.; Van de Vorst, A. Quantum yield of singlet oxygen production by xhantene derivatives. *Photochem. Photobiolo.* **1983**, *37* (3), 271-278. DOI: https://doi.org/10.1111/j.1751-1097.1983.tb04472.x.
(23) Redmond, R. W.; Gamlin, J. N. A compilation of singlet oxygen yields from biologically relevant molecules. *Photochem Photobiol* **1999**, *70* (4), 391-475. From NLM.
(24) Weynand, J.; Diman, A.; Abraham, M.; Marcélis, L.; Jamet, H.; Decottignies, A.; Dejeu, J.; Defrancq, E.; Elias, B. Towards the Development of Photo-Reactive Ruthenium(II) Complexes Targeting Telomeric G-Quadruplex DNA. *Chem. Eur. J.* **2018**, *24* (72), 19216-19227. DOI: doi:10.1002/chem.201804771. Bevernaegie, R.; Doix, B.; Bastien, E.; Diman, A.; Decottignies, A.; Feron, O.; Elias, B. Exploring the Phototoxicity of Hypoxic Active Iridium(III)-Based Sensitizers in 3D Tumor Spheroids. *J. Am. Chem. Soc.* **2019**, *141* (46), 18486-18491. DOI: 10.1021/jacs.9b07723.
(25) Gillard, M.; Weynand, J.; Bonnet, H.; Loiseau, F.; Decottignies, A.; Dejeu, J.; Defrancq, E.; Elias, B. Flexible RuII Schiff Base Complexes: G-Quadruplex DNA Binding and Photo-Induced Cancer Cell Death. *Chemistry – A European Journal* **2020**, *26* (61), 13849-13860, https://doi.org/10.1002/chem.202001409. DOI: https://doi.org/10.1002/chem.202001409 (acccessed 2021/02/08).

Tables of contents

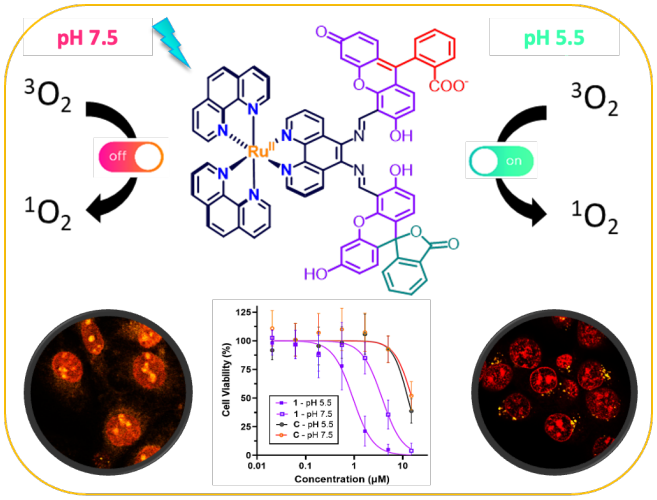

Developing pH-activatable PDT agents thanks to the combination of the $^1O_2$ photoproduction ability of Ru^{II} polypyridyl complexes with the great pH sensitivity of fluorescein.